membranes

MDPI

Article

Preparation and Properties of Polyaldehyde–Polyamine-Based Positively Charged Nanofiltration Membranes for Monovalent/Divalent Ion Separation

Kaiqiang Cao [1], Tong Sun [1], Shaoqi Zhang [1], Shuai Zhou [1], Yuanyuan Tang [1], Quangang Cheng [1], Zheng Cao [1], Zihao Zhao [1,2], Chuanjie Fang [3], Heba Abdallah [4], Eman S. Mansor [5], Baoku Zhu [1,3,*] and Ziran Zhu [1,*]

[1] ERC of Membrane and Water Treatment (MOE), China-Portugal Belt and Road Joint Laboratory on Advanced Materials, Department of Polymer Science and Engineering, Zhejiang University, Hangzhou 310058, China
[2] Hangzhou Super Elements Co., Ltd., Hangzhou 310018, China
[3] Center for Healthcare Materials, Life Health Research Center, Shaoxing Institute, Zhejiang University, Shaoxing 312099, China
[4] Chemical Engineering & Pilot Plant Department, Engineering Research Institute, New and Renewable Energy, National Research Centre, Dokki, Giza 12622, Egypt
[5] Water Pollution Research Department, Environment and Climate Change Research Institute, National Research Centre, Dokki, Giza 12622, Egypt
* Correspondence: zhubk@zju.edu.cn (B.Z.); hzzhuzr@zju.edu.cn (Z.Z.)

Abstract

Nanofiltration (NF) technology has emerged as a promising water treatment technology owing to its low energy consumption and high water flux. However, conventional negatively charged NF membranes are incapable of satisfying the demands of hard water softening, and severe membrane fouling still acts as a critical bottleneck limiting their practical application. Herein, a novel dual-polymer cross-linking strategy is developed to construct positively charged sieving layers on ultrafiltration substrates through a one-step coating and thermal curing approach, in which zwitterionic polyethyleneimine (QSPEI) and polyacrolein (PA) serve as dual building blocks. The interpenetrating covalent cross-linking network between QSPEI and PA macromolecules forms a compact and stable separation layer, enabling the successful fabrication of high-performance composite NF membranes. Under optimal preparation conditions, the obtained membrane exhibits a high $MgCl_2$ rejection of 95.1% and an excellent pure water permeance of 10.9 $L \cdot m^{-2} \cdot h^{-1} \cdot bar^{-1}$, while maintaining a high flux recovery rate of 91.0% against 100 ppm BSA fouling. The prominent antifouling performance, comparable to that of typical zwitterionic NF membranes, originates from the coexisting positive and negative charges on QSPEI chains induced by quaternization and sulfonation modification. Meanwhile, the dense cross-linked network endows the membrane with outstanding separation efficiency toward both monovalent and divalent cations. This work provides a feasible fabrication strategy for advanced NF membranes with synergistic separation and antifouling performance, possessing great application potential in water softening and ion separation.

Keywords: nanofiltration membranes; quaternary ammonium–sulfonation modification; polyethyleneimine; polyacrolein; fouling resistance

Check for updates

Academic Editor: Young Hoon Cho

Received: 21 September 2026
Revised: 15 October 2026
Accepted: 19 October 2026
Published: 23 October 2026

Copyright: © 2026 by the authors. Licensee MDPI, Basel, Switzerland. This article is an open access article distributed under the terms and conditions of the Creative Commons Attribution (CC BY) license.

1. Introduction

Compared with traditional water treatment technologies such as MF and UF, nanofiltration membranes have demonstrated significant practical value in fields such as wastew-

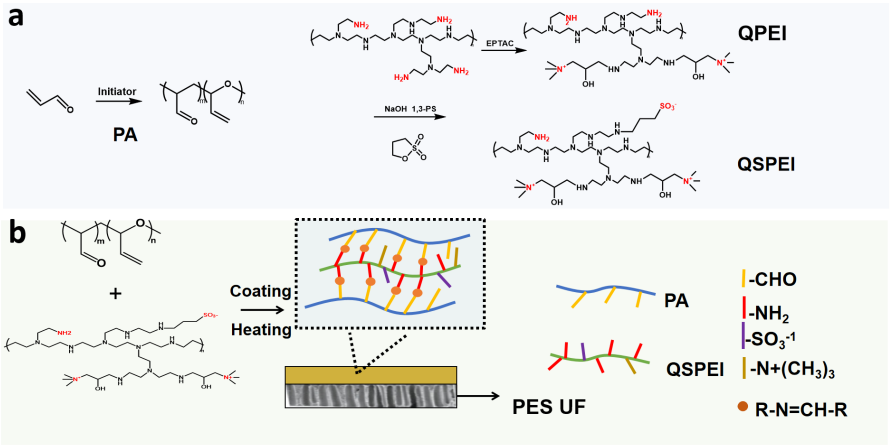
ater recovery and desalination, owing to their advantages of low energy consumption and high water permeance [1–3]. In practical applications, conventional nanofiltration membranes often suffer from low surface hydrophilicity, unsatisfactory charge stability and poor antifouling mechanisms. As a result, organic matter readily adsorbs onto the membrane surface, leading to fouling and rapid permeance decay, which severely limits membrane separation efficiency and long-term operational stability [4–6]. Consequently, the development of nanofiltration membranes that combine high salt-separation capability with excellent antifouling performance [7–9] has become a key research focus in the field of membrane separation, attracting increasing attention from researchers.

Positively charged nanofiltration membranes rely on the Donnan effect and size-sieving effect to efficiently remove divalent cations from water, and are of great value in fields such as hard water softening. Interfacial polymerization is currently the most widely used method for membrane preparation [10–12]. Yang Zhao et al. [13] synthesized the bis-quaternary-ammonium modifier MDTAB (1-methyl hydrazide-3,5-dibenzyl trimethyl ammonium bromide), which was grafted onto polyamide nanofiltration membranes through an amidation reaction between amino groups and acyl chloride groups on the membrane surface, so as to increase the surface positive-charge density and realize efficient Mg^{2+} rejection. Jun Xiang et al. [14] prepared QPEI by quaternizing PEI, and fabricated loose positively charged nanofiltration membranes via interfacial polymerization with TMC. The resultant membranes feature high permeate flux, and over 98% rejection for dyes and divalent cations, and can treat cationic-dye-containing wastewater with stable operation performance. Zhe Wang et al. [15] synthesized the tri-quaternary-ammonium monomer QPMDETA using PMDETA (pentamethyldiethylenetriamine) and 2-bromoethylamine hydrobromide, and modified PEI-based nanofiltration membranes by secondary interfacial polymerization. These modifications improved the surface positive-charge density and hydrophilicity of membranes, and achieved high permeate flux as well as excellent Mg^{2+} rejection. Nevertheless, interfacial polymerization still possesses inherent limitations. Its ultra-fast reaction kinetics can easily induce inhomogeneous membrane structures under minor process disturbances. Furthermore, the preparation relies on volatile organic solvents with low monomer utilization, which tends to bring about resource waste and environmental pollution. Therefore, non-interfacial-polymerization fabrication strategies have drawn increasing attention.

The one-step cross-linking coating method stands out as one of the most competitive alternatives to interfacial polymerization (IP). As reported in representative studies, glutaraldehyde (GA) is frequently employed as a cross-linking agent for nanofiltration membrane preparation owing to its high reactivity [16–18]. However, as a small-molecule aldehyde, GA is highly toxic and volatile, which means that it can easily cause secondary pollution [19,20]. In addition, multi-step coating suffers from cumbersome operation, uneven membrane thickness and poor batch-to-batch reproducibility [21].

In comparison, the one-step aqueous dual macromolecule cross-linking coating method has prominent advantages. With only one coating–curing cycle, the aqueous system is eco-friendly and safe, and the simple process can be easily scaled up. It allows flexible membrane structure regulation to minimize defects and mitigate coating inhomogeneity in multi-step procedures. However, limited by the types of available reactive macromolecules, substantial breakthroughs remain absent. Nevertheless, constrained by the limited variety of reactive macromolecules, no remarkable breakthrough has been achieved to date. With advances in polymer science, amino polymers combining functionality, high reactivity, easy accessibility and modifiability, such as PEI, poly(allylamine), and poly(vinylamine), can be fabricated at scale. Utilizing the amino groups in these macromolecules provides new opportunities for developing positively charged NF membranes

based on macromolecular coatings. Small-molecule cross-linkers such as GA can cross-link these amino polymers to form nanofiltration membranes [22,23]. However, significant challenges still remain regarding the structural homogeneity, water flux, and environmental performance during the fabrication of such nanofiltration membranes. By comparison with GA-like cross-linkers, macromolecular cross-linking agents are non-volatile under heat treatment, have low toxicity and possess a high cross-linking degree. In the membrane formation process, the homogeneous dispersion of macromolecules and higher viscosity in casting solutions make a coating more stabilizable and produce a denser membrane structure. Therefore, it is of great significance to synthesize macromolecular aldehyde cross-linking agents and fabricate polyamine-based positive NF membranes. Based on this background, this study proposes a strategy for fabricating positively charged NF membranes (PEI-PA) by cross-linking PEI with macromolecular aldehyde (poly(acrolein), PA) (Scheme 1). To overcome the fouling tendency generated by the inherent positive nature of amine units, the zwitterionic groups were also integrated into the NF membranes via a simple process. From these attempts, a novel and applicable preparation method should be expected for the preparation of novel positively charged NFMs.



Scheme 1. (**a**) Synthesis of PA and zwitterionic PEI; (**b**) preparation of nanofiltration membranes via cross-linking of PA and QSPEI.

2. Materials and Methods

2.1. Materials and Reagents

A PES UF membrane (MWCO = 20,000 Da) was purchased from Guo chu Chemical Co., Ltd. (Xiamen, China). Polyethyleneimine (PEI, Mw = 70,000 Da), 1,3-propanesultone (1,3-PS), and 2,3-epoxypropyltrimethylammonium chloride (EPTAC) were purchased from Sinopharm Chemical Reagent Co., Ltd. (Shanghai, China). Methanol, ethanol, diethyl ether, hydroxylamine hydrochloride, and ethyl acetate were obtained from Shanghai Aladdin Reagent Co. (Shanghai, China), and used without further purification. Hydrochloric acid (HCl), sodium hydroxide (NaOH), sodium chloride (NaCl), calcium chloride ($CaCl_2$), magnesium sulfate ($MgSO_4$), sodium sulfate (Na_2SO_4), magnesium chloride ($MgCl_2$), and bovine serum albumin (BSA) were all of analytical grade and purchased from Shanghai Chemical Reagent Co., Ltd. (Shanghai, China). Deionized water was used in all experiments.

2.2. Synthesis of and Characterization of Polyacrolein (PA)

Polyacrolein was prepared by the free-radical polymerization of acrolein monomer with 2,2′-azobis(2-(2-imidazolin-2-yl)propane) dihydrochloride as the initiator. The reaction was carried out at constant temperature under nitrogen protection. Upon the completion of

polymerization, the product was purified and dried to yield the final polyacrolein. Molecular weight and compositional analysis confirmed that the obtained polymer contained both aldehyde and vinyl groups. From the peak integrals of the –CHO signal (H_a, 9.75 ppm) and –CH=CH_2 signal (H_e, 6.52 ppm), the molar ratio of aldehyde moieties to vinyl moieties was calculated to be 47%:53%. In addition, the relative molecular weight of PA measured by gel permeation chromatography (GPC) is 25,000 g mol^{-1}. Detailed synthetic procedures and structural characterizations are available in previous literature [24].

2.3. Synthesis and Characterization of Modified PEIs

Based on the total amine value of PEI 70k (0.0147 mol·g^{-1}) determined by titration, PEI was subjected to either single quaternization modification or combined quaternization–sulfonation modification in this study; the preparation process is shown in Scheme 1. For the single quaternization modification, a 10.0 wt% PEI solution was prepared in methanol; EPTAC, equivalent to 20% of the total moles of amine groups in PEI, was added, and the mixture was reacted at 60 °C for 2 h to produce QPEI with a quaternization degree of 20%. For the combined modification, the quaternization pretreatment was first carried out under the same conditions; an excess of flaky NaOH was then added to neutralize protonated amino groups in the system and activate the remaining amino groups. Subsequently, 1,3-PS, equivalent to 20% of the total number of moles of PEI, was added, and the reaction was continued for 3 h at 60 °C. Finally, the modified product, QSPEI, was obtained following purification with ethyl acetate, centrifugation and drying.

To determine the chemical structure of PEI, Fourier-transform infrared spectroscopy (FTIR, Bruker Vector-22, Ettlingen, Germany) and ^{1}H nuclear magnetic resonance spectroscopy (^{1}H NMR, Bruker Avance 500, Germany) were employed to characterize the structure of the modified PEI.

2.4. Preparation of Nanofiltration Membranes

First, the PES substrate was immersed in deionized water at 25 °C and subjected to ultrasonic treatment for 15 min to clean the surface. Subsequently, the various modified PEI aqueous solutions described above were mixed with an equal volume of PA alcohol–water solution; HCl was added prior to mixing to adjust the pH, and the substrate was secured to an 8 cm × 8 cm PTFE plate-and-frame assembly, ensuring that its surface remained flat. The mixture of modified PEI and PA was applied to the substrate membrane by spraying, with a coating volume of 3.6 mL (1.97 g/m^2). Finally, the membrane was heat-treated for 10 min in an oven at 60 °C. The prepared nanofiltration membranes were stored in deionized water for later use. The membrane prepared from PEI and PA was designated as M_0 for use as a control; the membrane prepared from quaternized PEI and PA was designated as M_Q; and the membrane prepared from quaternized and sulfonated PEI and PA was designated as M_{QS}.

2.5. Chemical Characterization of Membranes

To identify the chemical composition of the membrane surface, the membrane surface was analyzed using attenuated total reflection Fourier-transform infrared spectroscopy (ATR-FTIR, Nicolet 6700, Thermo Fisher Scientific Inc., Waltham, MA, USA) and X-ray photoelectron spectroscopy (XPS, K-Alpha, Thermo Fisher Scientific Inc., USA). FESEM (Hitachi S-4800) and AFM (Atomic Force Microscopy, Cypher ES, Oxford Instruments Asylum Research, Inc., Santa Barbara, CA, USA) were used to examine the structure and morphology of the composite nanofiltration separation layer, as well as the surface roughness of the membrane. A contact angle-measuring instrument (OCA20, Data Physics Instruments GmbH, Filderstadt, Germany) was used to test the hydrophilicity of the

membrane surface. A solid-surface zeta potential analyzer was used to determine the zeta potential of the composite membrane surface within the pH range of 3.0–10.0.

2.6. Pore Size Characterization of NF Membranes

Under conditions of 25 °C and 4 bar, PEG with increasing molecular weights was used as the feed solution to test its rejection. The MWCO of the membrane refers to the molecular weight corresponding to a PEG retention rate (R_{PEG}, calculated using Equation (1)) of 90%. The PEG concentration was measured using a total organic carbon analyzer (TOC-V, Shimadzu, Kyoto, Japan). The Stokes' diameter (ds, nm) of PEG was calculated using Equation (2), and the pore size distribution of the nanofiltration membrane was evaluated using the probability density function in Equation (3) [25–27], where dp (nm) is the pore size, σp is the ratio of solute diameters at retention rates of 84.13% and 50%, and μp (nm) is the mean effective diameter corresponding to the size of a neutral solute at a rejection of 50%.

$$R_{PEG} = \left(1 - \frac{TOC_{permeate}}{TOC_{feed}}\right) \times 100\% \quad (1)$$

$$d_s = 33.46 \times 10^{-3} \times M^{0.557} \quad (2)$$

$$\frac{dR(dp)}{ddp} = \frac{1}{\sqrt{2\pi}dpln\sigma_p} exp\left[-\frac{(lndp - ln\mu_p)^2}{2(ln\sigma_p)^2}\right] \quad (3)$$

2.7. Membrane Separation Performance Tests

The separation performance of the nanofiltration membrane was tested using an ultrafiltration cup. The separation operating pressure was maintained at 4 bar throughout, the feed solution was kept at a constant temperature of 25 °C, and the stirring speed of the magnetic stirrer in the ultrafiltration cup was fixed at 600 rpm. Prior to testing, the nanofiltration membrane was pre-pressurized with ultrapure water at 5 bar for 1 h to ensure membrane stability. The water permeability was calculated using Equation (4) [28–30].

$$Jw = \Delta V/(PA\Delta t) \quad (4)$$

In the formula, Jw represents the water permeability ($L \cdot m^{-2} \cdot h^{-1} \cdot bar^{-1}$), ΔV denotes the volume of permeate (L), P refers to the operating pressure during the test (bar), A is the effective membrane area (1.256×10^{-3} m^2), and Δt is the filtration time (h). The retention rate of nanofiltration membranes for divalent salts was tested using the same apparatus. The salt concentration throughout the test was 1000 ppm.

The salt retention rate of a nanofiltration membrane is calculated using Equation (5) [31,32].

$$R = (1 - C_p/C_f) \times 100\% \quad (5)$$

where C_p represents the concentration of the permeate, whilst C_f represents the concentration of the solute in the feed. The solutions were analyzed for conductivity (DDS-11A, Shanghai Leizhi Instrument Co., Ltd., Shanghai, China). Each membrane was tested three times, and the average value was taken as the result.

2.8. Antifouling Performance Test

First, the membrane was pre-compacted with deionized water for 5 h, followed by testing with a 100 ppm BSA solution for 5 h. This procedure is defined as one filtration cycle. Each nanofiltration membrane will undergo 2.5 filtration cycles. After each cycle, the nanofiltration membrane is rinsed with deionized water for 1 h. The relative flux recovery (Jr) is calculated using the following Equation (6) [33,34]:

$$J_r = J_t/J_0 \quad (6)$$

Here, J_0 and J_t represent the permeability at the start of filtration and the hourly permeability, respectively.

2.9. Stability Test of Nanofiltration Membranes

The ultrafiltration cup was used to evaluate the membrane stability. For the long-term stability test, the operating pressure was set at 4 bar. After 1 h of pre-pressurization, the permeate flux and rejection were calculated according to Equations (4) and (5). The membrane performance was then measured every 20 h. For the pressure resistance test, the operating pressure was gradually increased from 1 bar to 5 bar. The system was stabilized for 30 min at each pressure, and the variations in pure water flux and rejection were recorded. For the backwashing test, after the membrane was pre-pressurized and stabilized at 4 bar, backwashing tests were carried out with the pressure increasing stepwise from 1 to 5 bar, and the changes in pure water flux and salt rejection were recorded.

3. Results

3.1. Composition of Modified PEIs

From the FTIR spectrum in Figure 1a, QSPEI exhibits strong absorption peaks at 1185 cm^{-1} and 1037 cm^{-1}, confirming the successful introduction of the $–SO_3^-$ group. As shown in the ^1H NMR spectra in Figure 1b–d, QPEI exhibits a methyl proton absorption peak at 3.30 ppm assigned to the $–N^+(CH_3)_3$ group and a methylene proton absorption peak at 4.17 ppm assigned to the –CH(OH) group, confirming the successful introduction of the-$N^+(CH_3)_3$ group. For QSPEI, in addition to the proton absorption peaks mentioned above, proton absorption peaks originating from the $–(CH_2)_3SO_3^-$ methylene group were also observed at 2.02, 3.07, and 3.62 ppm, further confirming the successful introduction of the $–SO_3^-$ group.

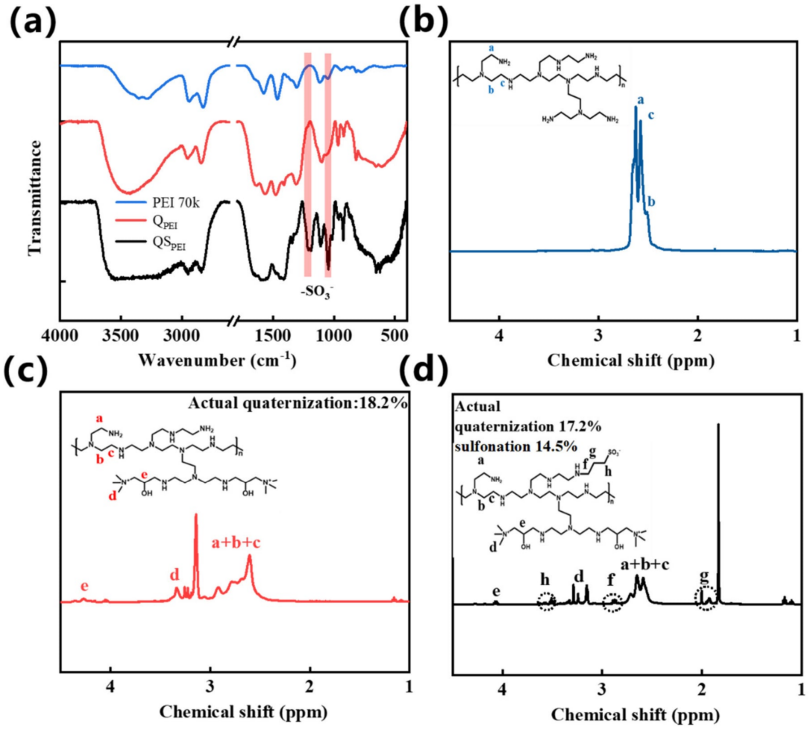


Figure 1. (**a**) FTIR spectra and ^1H NMR spectra of (**b**) PEI 70k; (**c**) quaternized PEI; and (**d**) quaternized and sulfonated PEI.

3.2. Optimization for Preparing Nanofiltration Membranes

To optimize the performance of the nanofiltration membrane, optimization was performed with respect to concentration, reaction temperature and degree of quaternization. Figure 2a shows the effect of polyacrolein (PA) concentration; as the concentration increases, the degree of cross-linking increases and the membrane layer structure becomes denser. When the PA concentration reaches 0.20 wt%, the salt rejection stabilizes at 98 ± 0.3%. Figure 2b presents the influence of modified PEI concentration on the interfacial cross-linked network. At a concentration of 0.50 wt%, sufficient cross-linking between the PEI segments and PA formed a Schiff base separation layer with ideal nanofiltration performance. Under this condition, the rejection reaches 98.9%, while permeance remains at 10.9 $L \cdot m^{-2} \cdot h^{-1} \cdot bar^{-1}$. Figure 2c illustrates the effect of reaction temperature on membrane separation performance, with optimal conditions achieved at 60 °C. Figure 2d shows the effect of quaternization degree on the separation membrane's performance; when the quaternized level of PEI was increased to 20%, the retention rate of $MgCl_2$ rose to 98.7% owing to the Donnan effect. Beyond this threshold, the retention rate decreased significantly due to an increase in defects in the cross-linked network resulting from a reduction in the concentration of active primary amine groups. Therefore, the combination of a PA concentration of 0.20 wt%, a modified PEI concentration of 0.50 wt%, and a reaction temperature of 60 °C was determined to be the optimal set of parameters. All subsequent test membranes were prepared under these conditions.

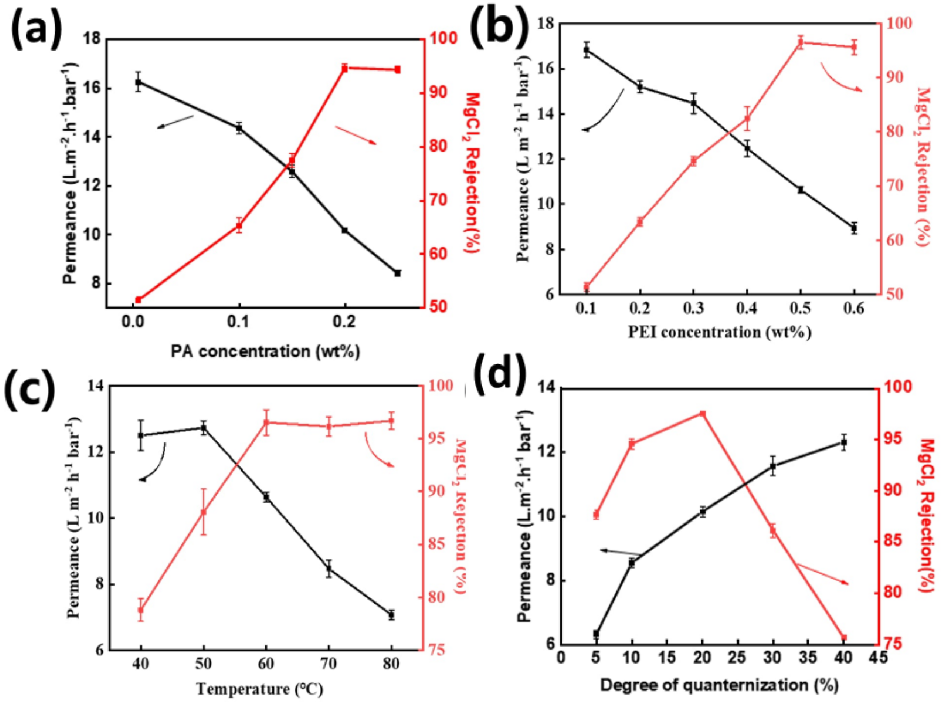


Figure 2. Effects of (**a**) PA concentration, (**b**) PEI concentration, (**c**) reaction temperature and (**d**) degree of quaternization on the separation performance of the NF membranes.

3.3. Morphologies and Composition of Nanofiltration Membranes

Characterization of the membrane microstructure via SEM, as shown in Figure 3, reveals the structure–property relationship between surface morphology and chemical modification. The top panel of Figure 3 shows that, compared with the well-defined porous structure of the pristine PES substrate, the surface porosity of the modified nanofiltration membrane is significantly reduced, confirming the formation of an intact selective layer atop the substrate membrane. The surface of the unmodified sample M_0 exhibits a smooth and

dense structure, which is attributed to the high-density Schiff base cross-linking between PEI and PA molecular chains. Following quaternary ammonium modification, the surface of the M_Q membrane exhibits discretely distributed spherical protrusions, with a significantly increased roughness; this is attributed to the quaternization process weakening the cross-linking strength of the PEI molecules, thereby increasing the spacing between polymer chains and inducing a topological restructuring. The M_{QS} membrane, which undergoes further sulfonation modification of PEI, exhibits a more complex surface morphology. Conformational contraction of the modified PEI segments alters the stacking pattern of molecular chains, thereby generating a rough, wrinkled membrane interface. These results demonstrate that the packing arrangement of polymer chains can be effectively tuned via chemical functional group modification, enabling the precise engineering of micro- and nanostructures on the membrane surface.

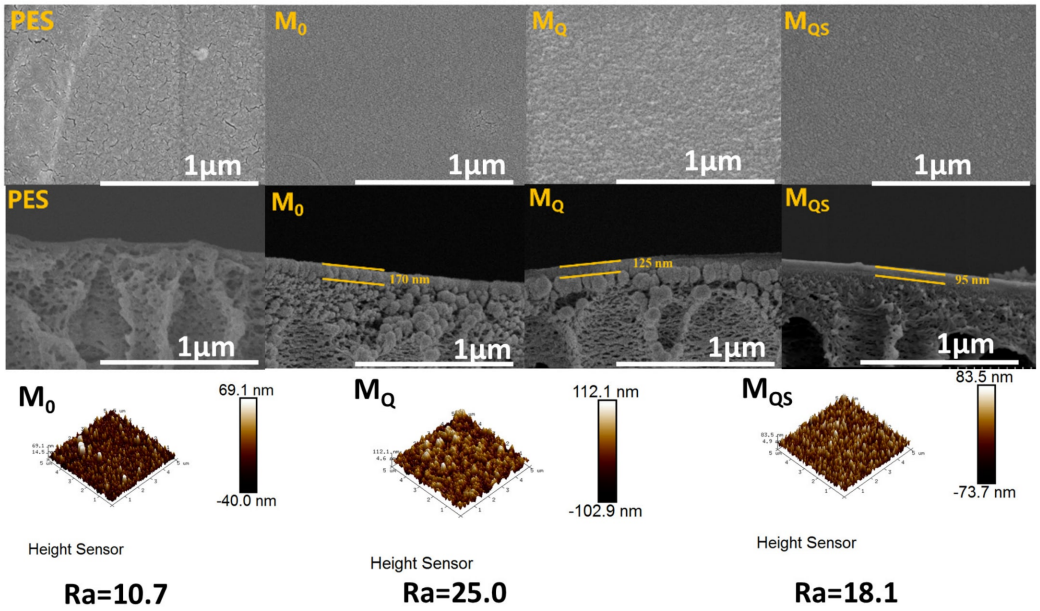


Figure 3. SEM surface and cross-sectional morphologies of the substrate and NF membrane, as well as the surface roughness of the NF membrane.

To probe the active layer thickness originating from the cross-linking of differently modified PEI samples, cross-sectional SEM images are displayed in the second row of Figure 3. The M_0 film exhibits the greatest thickness of 170 nm, while the M_Q and M_{QS} membranes show thicknesses of 125 nm and 95 nm, respectively. For the M_0, M_Q and M_{QS} membranes, the thickness primarily depends on the extent of the reaction between the amine groups and the aldehyde groups in the PA. In the case of M_0, PEI cross-links fully with PA, whereas for M_Q, the reduction in reactive amine groups results in a lower degree of cross-linking, leading to a decrease in thickness. For M_{QS}, the further depletion of reactive amine groups further lowers the membrane thickness to 95 nm. The weakened reaction between PEI and PA reduces polymer deposition on the substrate, thereby thinning the resultant selective layer.

Figure 4a shows the XPS analysis of elements on the membrane surface. Distinct N 1s (399.7 eV), C 1s (284.8 eV) and O 1s (531.6 eV) peaks are observed on the surfaces of all nanofiltration membranes, while only the PES and M_{QS} membranes exhibited a peak at 170.2 eV corresponding to the S 2p peak. Taken together, these results confirm the formation of a separation layer on the PES substrate.

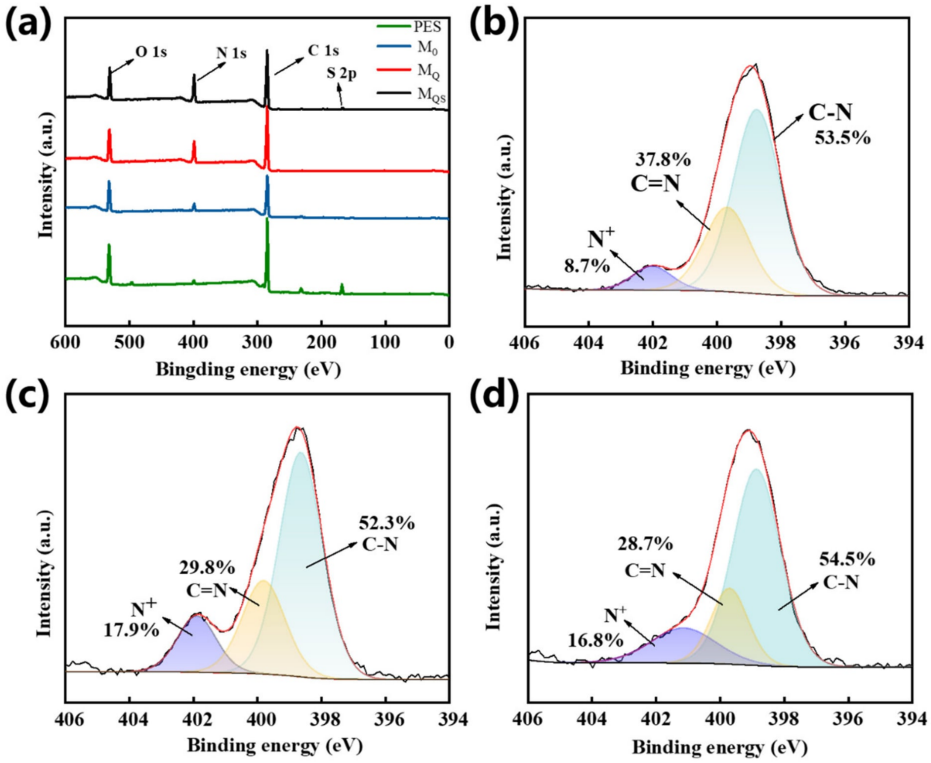


Figure 4. (**a**) XPS spectra of PES substrate and NF membranes; N 1s XPS spectra of (**b**) M_0 membrane; (**c**) M_Q membrane; and (**d**) M_{QS} membrane.

Figure 4b–d show the high-resolution N 1s XPS spectra of the nanofiltration membranes. As shown, the peak at 398.9 eV originates from the C–N bond in PEI. In all nanofiltration membranes, the C=N bond appears at 399.7 eV, confirming the Schiff base reaction between the amine and aldehyde groups [35–37]. Furthermore, the peak at 401.8 eV corresponds to $–N^+$, which is attributable to the protonation effect of the amine and $–NH_4^+$ groups resulting from the modification of the nanofiltration membranes. Spectral analysis gives the content of $–N^+$, which varies from 8.7% to 17.9% and 16.8% as PEI is modified, consistent with the theoretical degree of PEI modification.

3.4. Surface Hydrophilicity and Charge State

As shown in Figure 5a, the PES substrate exhibits a contact angle of 65.9°, indicating its relatively hydrophobic nature. Upon functionalization, the M_0 membrane shows a markedly reduced contact angle of 49.7°, verifying that the introduction of amine and aldehyde functional groups effectively improves surface hydrophilicity. As quaternization proceeds, the surface contact angles of M_Q and M_{QS} membranes decrease to 42.6° and 33.7°, respectively. This is mainly attributed to the synergistic effect of $–NH_4^+$ and $–SO_3^-$ groups. On the one hand, these ionic groups with strong hydration capacity markedly improve surface wettability [38–40]. On the other hand, the elevated density of functional groups further lowers contact angle values by increasing surface polarity. The high density of ionic groups on the M_{QS} membrane surface endows it with the optimal hydrophilic performance.

Figure 5b shows that the pristine PES membrane exhibits a zeta potential of −22.0 mV at pH 6.4. In contrast, all modified nanofiltration membranes present positively charged surfaces. This characteristic stems from the protonation of amine groups in PEI to form $-NH_3^+$, as well as the generation of $-NH_4^+$ groups via PEI quaternization, both of which endow the membrane surfaces with positive electrical properties [41–43]. Consequently, M_Q exhibits the highest zeta potential among all nanofiltration membranes. With the introduction of modified PEI, a smaller number of unreacted amine groups from the mixed

amines remain in the selective layer and gradually exhibit a strong positive charge. At pH 6.4, the zeta potentials of M_0, M_Q and M_{QS} are 4.1, 17.5 and 11.2 mV, respectively, confirming the presence of a greater positive charge on the membrane surface. In the case of M_{QS}, as the degree of modification increased further, negatively charged $-SO_3^-$ groups appeared, causing its zeta potential to decrease to 11.2 mV.

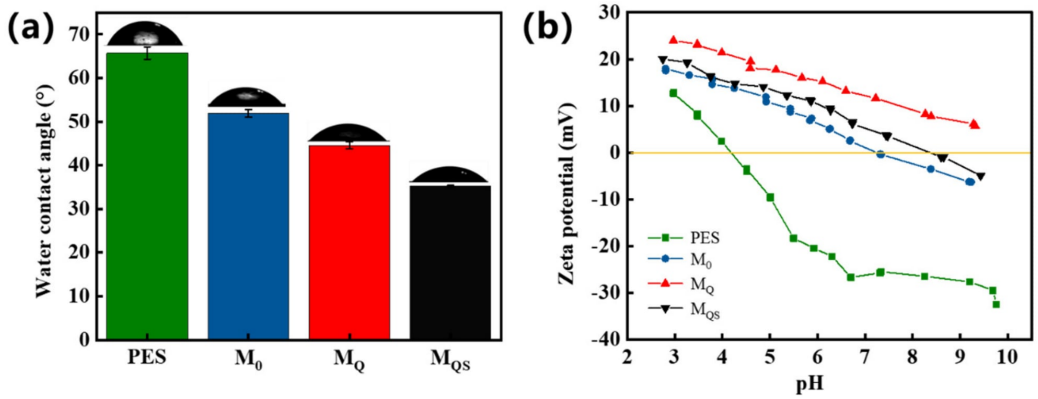


Figure 5. (**a**) shows the contact angles of all nanofiltration membranes; (**b**) shows the zeta potential curves of all nanofiltration membranes.

3.5. Nanofiltration Membrane Performance

3.5.1. Molecular Weight Cut-Off and Pore Size Distribution

Figure 6a and 6b display the rejection of nanofiltration membranes toward five PEG solutes of different molecular weights and the pore size distributions of the corresponding membranes, respectively. The MWCO values of the M_0, M_Q, and M_{QS} membranes are 376 Da, 590 Da, and 462 Da, respectively. Based on the probability density function, their mean pore diameters are calculated to be 0.252 nm, 0.565 nm, and 0.437 nm, respectively. The M_0 membrane exhibits the smallest pore size because PA with abundant aldehyde groups forms a dense cross-linked network with PEI, which effectively reduces the pore diameter. For M_Q and M_{QS} membranes, the pore size increases gradually with PEI modification, which is consistent with the decreased cross-linking degree of the selective layer. Supplementary note: The molecular size corresponding to 50% rejection is estimated by extrapolation from the logistic fitting curve of PEG rejection data. This extrapolated value is only used for pore size distribution calculation, and the obtained pore size distribution represents merely estimated equivalent pore information rather than the absolute real physical pore size of the membrane.

The M_0 membrane has the smallest pore diameter, as PA possesses a high aldehyde group density, which allows for dense cross-linking with PEI, thereby resulting in a small pore diameter. For the M_Q and M_{QS} membranes, the pore diameter tends to increase with PEI modification, which is consistent with the reduced cross-linking degree of the separation layer. Following modification, fewer amine groups participate in the Schiff reaction, reducing the degree of cross-linking between PEI and PA. At the same time, the membrane pore size increases due to the modification and the formation of a looser network structure. In quaternized nanofiltration membranes, the mutual repulsion between PEI chains causes the chain segments to adopt an extended conformation, resulting in increased PA between chain segments after film formation and consequently larger membrane pore sizes. For M_{QS}, the introduction of sulfonic acid groups introduces electrostatic attraction, leading to a reduction in the size of the modified PEI and the formation of shrinkage pores in the membrane, thereby reducing the pore size.

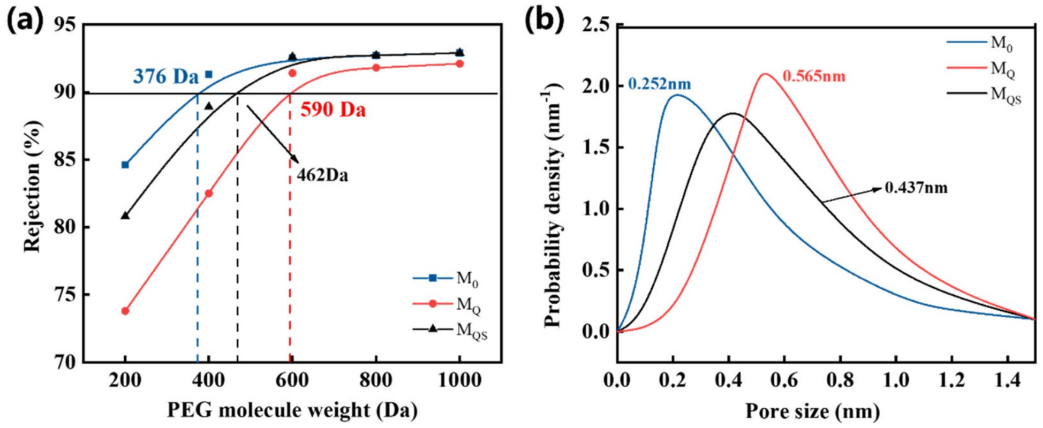


Figure 6. (**a**) shows the rejection rates of the nanofiltration membrane for five types of PEG; (**b**) shows the corresponding pore size distribution.

3.5.2. Permeability, Salt Separation and Antifouling Performance

As shown in Figure 7a, the pure water permeance of the unmodified M_0 membrane was 4.1 $L \cdot m^{-2} \cdot h^{-1} \cdot bar^{-1}$. After modification, the permeance of the M_Q and M_{QS} membranes increased to 7.8 and 10.9 $L \cdot m^{-2} \cdot h^{-1} \cdot bar^{-1}$, respectively, which are 1.9 and 2.7 times that of the M_0 membrane. This increase in permeance stems from the synergistic effect of multiple factors: first, the modification process reduced the thickness of the separation layer, thereby lowering mass transfer resistance; second, the reduced cross-linking degree between PEI and PA led to an increase in network pore size; third, the electrostatic repulsion effect of the quaternary ammonium segments promoted the extension of polymer chains, forming more open mass transfer channels; and finally, the enhanced surface hydrophilicity and increased surface roughness jointly facilitated the transport of water molecules. These structural optimizations enabled the modified membrane to exhibit markedly improved permeation performance.

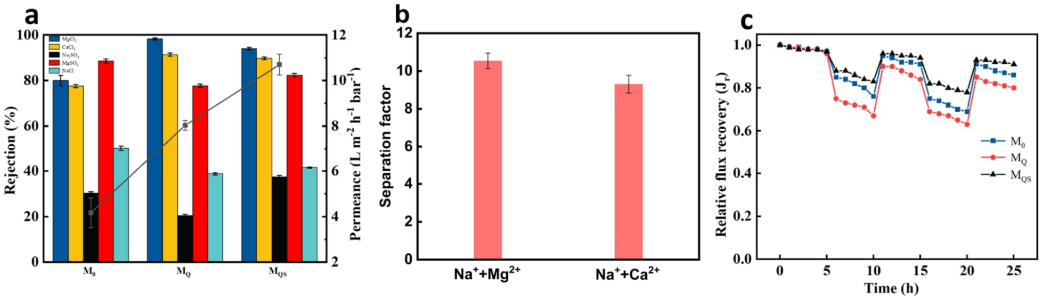


Figure 7. (**a**) Water permeance and $MgCl_2/CaCl_2/MgSO_4/NaCl/Na_2SO_4$ rejection performance of the three NF membranes; (**b**) separation factor performance of the membrane for Na^+/Mg^{2+} and Na^+/Ca^{2+} separation; (**c**) antifouling performance of various membranes.

Five typical inorganic salts were used to evaluate the separation performance of the prepared membranes. As shown in Figure 7a, for all the as-prepared nanofiltration membranes, the salt rejections are ranked as $Na_2SO_4 < NaCl < MgSO_4 < CaCl_2 < MgCl_2$, which is consistent with the characteristics of positively charged membranes. For $MgCl_2$, $CaCl_2$ and NaCl, the retention order is due to the size exclusion [44–46]. The hydration radii of Mg^{2+} (0.428 nm) and Ca^{2+} (0.412 nm) are greater than that of Na^+ (0.332 nm), and positively charged membranes exert stronger electrostatic repulsion on divalent cations than on monovalent cations; consequently, the retention rates of $MgCl_2$ and $CaCl_2$ are significantly higher than that of NaCl [47,48]. As the hydration radius of Mg^{2+} is larger than that of Ca^{2+}, the rejection of $MgCl_2$ is correspondingly higher due to the size-exclusion

effect. Furthermore, the divalent SO_4^{2-} anion partially screens the positive charges on the membrane surface, which greatly affects the salt rejection. Compared with Cl^-, SO_4^{2-} is more strongly attracted to the positively charged membrane; consequently, SO_4^{2-} can easily pass through the membrane, thereby reducing the rejection of salts containing divalent anions (i.e., $MgSO_4$ < $MgCl_2$, Na_2SO_4 < NaCl).

The ion rejection performance of membrane materials shows a significant correlation with their surface charge characteristics and pore size distribution. The data in Figure 7a show that the $MgCl_2$ rejections of the three membranes—M_0, M_Q and M_{QS}—are 80.5%, 98.9% and 95.1%, respectively, whilst the $CaCl_2$ rejections are 77.6%, 91.4% and 89.7%, respectively. This phenomenon is closely related to the charge density of the -NH_3^+ groups on the membrane surface; the M_Q membrane, possessing the highest density of -NH_3^+ groups, exhibits the highest zeta potential and achieves the highest rejection for divalent cations via the Dohan effect. For $MgSO_4$, the M_0 membrane exhibits a rejection of 88.6%, whilst those of the M_Q and M_{QS} membranes decrease to 77.7% and 82.3%, respectively. This is attributed to the gradual variations in their pore size: the pore size of the M0 membrane (0.252 nm) is smaller than the hydrated ionic radius of Mg^{2+} and SO_4^{2-} (0.379 nm), and high rejection is achieved primarily through size-exclusion mechanisms, whereas the increased pore sizes of the modified membranes (M_Q: 0.565 nm, M_{QS}: 0.437 nm) lead to the enhanced permeation of some ions. In addition, the separation performance of the M_{QS} was tested in mixed solutions of NaCl and $CaCl_2$, as well as NaCl and $MgCl_2$. The separation factors were 10.54 and 9.31, respectively. The membrane showed an excellent rejection capability toward divalent cations and could achieve the separation of monovalent and divalent ions.

In this study, a composite nanofiltration membrane bearing both quaternary ammonium and sulfonate groups was successfully fabricated via the amphoteric ionization of PEI. Given that increased surface charge density and roughness may exacerbate fouling risk, the antifouling performance of the modified membranes was systematically investigated. The sharp drop in relative flux in Figure 7c corresponds to the fouling stage. During BSA filtration, BSA molecules gradually deposit on the membrane surface to form a reversible cake layer, which increases the hydraulic resistance and reduces the permeate flux. The subsequent flux recovery corresponds to the hydraulic rinsing stage. After BSA filtration, the membrane surface is rinsed with cross-flow deionized water. The loosely deposited BSA cake is stripped under fluid shear force, the additional hydraulic resistance decreases, and the relative flux is restored.

The flux recovery rate of the M_0 membrane was 82.1%, whilst that of the quaternized M_Q membrane dropped to 78.2% due to enhanced contaminant adsorption arising from the accumulation of positive surface charges. The sulfonated M_{QS} membrane exhibited the highest flux recovery rate of 91.0%; this improvement in fouling resistance stems from an amphoteric effect: the surface $-SO_3^-$ groups effectively inhibit contaminant adhesion by forming a hydration layer [49–51], whilst the membrane maintains high cation rejection. This membrane material, which integrates excellent fouling resistance and selective separation performance, possesses great engineering potential for long-term water treatment applications.

3.5.3. Stability Nanofiltration of Membranes

As shown in Figure 8a, during long-term operation, the membrane flux decreases while the salt rejection remains nearly unchanged. This indicates that the membrane skin layer is not damaged and the charge density stays constant during long-term operation, demonstrating the favorable long-term stability of the membrane. Figure 8b presents the membrane pressure resistance performance. As the operating pressure increases, the water flux of the M_{QS} membrane increases linearly, whereas the $MgCl_2$ rejection remains stable,

demonstrating outstanding pressure tolerance and structural stability. Figure 8c shows the interfacial bonding strength between the selective layer and PES substrate evaluated via back-flushing tests. After back-flushing at 1 bar, the water permeability and $MgCl_2$ rejection of M_{QS} remained almost unchanged. Further elevation of the back-flushing pressure did not cause obvious variations in either permeance or rejection. Even at a high back-flushing pressure of 5 bar, the $MgCl_2$ rejection remained above 96%, confirming the robust interfacial adhesion between the selective layer and PES substrate. This excellent structural stability mainly originates from covalent bonding formed by nucleophilic substitution between the amino groups of the coating layer and the aryl ether moieties of the PES substrate, which endows the composite membrane with superior mechanical and structural stability.

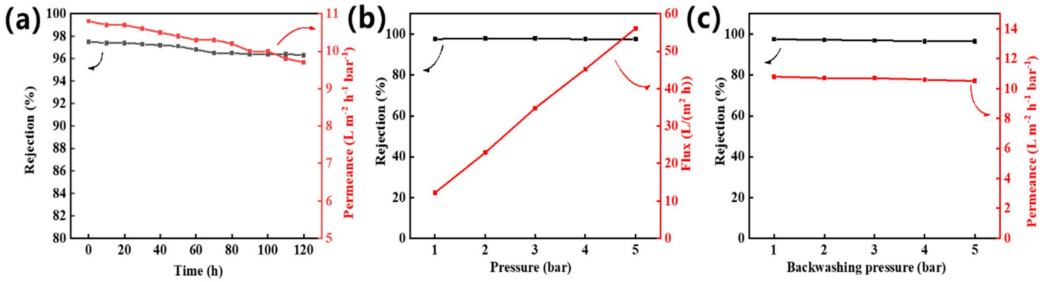


Figure 8. (**a**) Long-term stability of M_{QS} membrane under a certain operation time. Test conditions: $MgCl_2$ concentration = 1000 ppm, 25 °C, pH = 6.5, 4 bar. (**b**) The water flux and rejection of the M_{QS} membrane with different pressures ($MgCl_2$ concentration = 1000 ppm). (**c**) $MgCl_2$ rejection and permeance of M_{QS} membrane after backwashing for 30 min under different pressures.

4. Conclusions

The ionization of PEI enhances the interchain repulsion between PEI molecular chains. The cross-linked nanofiltration membrane accordingly presents a thinner surface separation layer and larger pore size. Meanwhile, the introduction of ionic groups significantly improves the hydrophilicity of the membrane surface, which further boosts the water permeation flux. Compared with the unmodified control membrane, nanofiltration membranes cross-linked with quaternized and zwitterionized PEI deliver improved water permeability and higher rejection rates for $CaCl_2$ and $MgCl_2$. For nanofiltration membranes fabricated via cross-linking zwitterionic PEI with polyacrolein, the mixed ionic groups on the membrane surface endow the membrane with typical zwitterionic characteristics and outstanding antifouling performance. This membrane achieves a $MgCl_2$ rejection of 95.1%, a water permeance of 10.9 $L \cdot m^{-2} \cdot h^{-1} \cdot bar^{-1}$, and a flux recovery rate of 91.0% during the filtration of a 100 ppm BSA solution. It exhibits great potential for the separation of monovalent and divalent cations as well as for antifouling applications. Moreover, the membrane maintains stable nanofiltration performance during long-term operation and forward/reverse flushing tests. These superior properties endow the fabricated nanofiltration membrane with promising practical application prospects in organic pollutant removal and hard water softening.

Author Contributions: Conceptualization, S.Z. (Shaoqi Zhang), S.Z. (Shuai Zhou), Z.C. and Z.Z. (Zihao Zhao); Methodology, K.C., Y.T. and Q.C.; Formal analysis, K.C.; Investigation, K.C. and T.S.; Resources, B.Z.; Writing—original draft, K.C.; Writing—review & editing, B.Z. and Z.Z. (Ziran Zhu); Visualization, K.C.; Supervision, B.Z.; Project administration, C.F., H.A., E.S.M., B.Z. and Z.Z. (Ziran Zhu); Funding acquisition, C.F., H.A., E.S.M., B.Z. and Z.Z. (Ziran Zhu). All authors have read and agreed to the published version of the manuscript.

Funding: This research was funded by [the National Key Research and Development Program of China], grant number [2025YFE0121100]; [the Science, Technology & Innovation Funding Authority

under Egypt-China Cooperation Program grant], grant number [ID 50335] and [the Fundamental Research Funds for the Central Universities], grant number [226-2026-00036].

Data Availability Statement: The original contributions presented in this study are included in the article. Further inquiries can be directed to the corresponding author(s).

Conflicts of Interest: Zihao Zhao was employed by the company Hangzhou Super Elements Co., Ltd. The remaining authors declare that the research was conducted in the absence of any commercial or financial relationships that could be construed as a potential conflict of interest.

References

1. Ahmad, N.N.R.; Mohammad, A.W.; Mahmoudi, E.; Ang, W.L.; Leo, C.P.; Teow, Y.H. An Overview of the Modification Strategies in Developing Antifouling Nanofiltration Membranes. *Membranes* **2022**, *12*, 1276. [CrossRef] [PubMed]
2. Liu, L.; Lan, H.; Cui, Y.; Tang, Q.; Bai, J.; An, X.; Sun, M.; Liu, H.; Qu, J. A Janus membrane with electro-induced multi-affinity interfaces for high-efficiency water purification. *Sci. Adv.* **2024**, *10*, eadn8696. [CrossRef] [PubMed]
3. Gan, B.; Peng, L.E.; Liu, W.; Zhang, L.; Wang, L.A.; Long, L.; Guo, H.; Song, X.; Yang, Z.; Tang, C.Y. Ultra-permeable silk-based polymeric membranes for vacuum-driven nanofiltration. *Nat. Commun.* **2024**, *15*, 8656. [CrossRef] [PubMed]
4. Yu, R.; Zhang, H.; Gan, Y.; Wang, X.; Wang, T.; Li, J.; Shi, M.; Dong, C.; Wu, F. One-step hydrophilic network for simultaneous boost in scaling prone cation removal and resistance to organic fouling of nanofiltration membranes. *J. Environ. Chem. Eng.* **2026**, *14*, 124038. [CrossRef]
5. Ebrahimi, M. Polymeric Nanofiltration Membranes with Enhanced Hydrophilic, Morphological, Transport, and Antifouling Properties—A Review. *Polymers* **2026**, *18*, 2066. [CrossRef] [PubMed]
6. Hu, Z.; Tian, K.; Li, L.; Dai, H.; Peng, Z.; Yin, Z.; Yang, W. Broad-spectrum rejection of emerging organic contaminants with different structures and properties from complex water matrices by a chlorine-resistant Janus nanofiltration membrane. *Chem. Sci.* **2026**, *17*, 1137–1150. [CrossRef] [PubMed]
7. Yadav, S.; Ibrar, I.; Samal, A.K.; Altaee, A.; Déon, S.; Zhou, J.; Ghaffour, N. Preparation of fouling resistant and highly perm-selective novel PSf/GO-vanillin nanofiltration membrane for efficient water purification. *J. Hazard. Mater.* **2022**, *421*, 126744. [CrossRef] [PubMed]
8. Zinadini, S.; Zinatizadeh, A.A.L.; Rahimi, M.; Vatanpour, V. Magnetic field-augmented coagulation bath during phase inversion for preparation of $ZnFe_2O_4/SiO_2$/PES nanofiltration membrane: A novel method for flux enhancement and fouling resistance. *J. Ind. Eng. Chem.* **2017**, *46*, 9–18. [CrossRef]
9. Song, J.; Xu, D.; Han, Y.; Zhu, X.; Liu, Z.; Li, G.; Liang, H. Surface modification of FeIII-juglone coating on nanofiltration membranes for efficient biofouling mitigation. *Water Res.* **2023**, *247*, 120795. [CrossRef] [PubMed]
10. Zhou, C.; Chen, E.; Yuan, J.; Liu, Z.; Jiao, Y.; Lin, H.; Xu, Y.; Shen, L. Buffer-regulated interfacial polymerization of tannic acid for high-performance polyester nanofiltration membranes. *J. Membr. Sci.* **2026**, *757*, 125887. [CrossRef]
11. Zhang, H.; Wu, J.; Cao, X.; Guo, J.; Elimelech, M.; Wang, Y. Suppressing Polyamide Crystallization Unlocks Ultrapermeable and Highly Selective Nanofiltration Membranes. *Nat. Commun.* **2026**, *17*, 10481. [CrossRef] [PubMed]
12. Pan, Y.; Tu, C.; Li, X.; Gao, L.; Xu, B.; Zhang, W.-H.; Meng, H. Facile fabrication of COF nanofiltration membranes via acetic acid-catalyzed interfacial polymerization. *J. Membr. Sci.* **2025**, *732*, 124269. [CrossRef]
13. Zhao, Y.; Wu, T.; Wang, Y.; Feng, Z.; Cheng, L.; Zheng, Y.; Wang, H.; Xu, K.; Zhang, R.; Jiang, Z. Highly positively charged nanofiltration membrane through bis-quaternary ammonium modification for Li^+/Mg^{2+} separation. *Desalination* **2025**, *603*, 118659. [CrossRef]
14. Xiang, J.; Li, H.; Hei, Y.; Tian, G.; Zhang, L.; Cheng, P.; Zhang, J.; Tang, N. Preparation of highly permeable electropositive nanofiltration membranes using quaternized polyethyleneimine for dye wastewater treatment. *J. Water Process Eng.* **2022**, *48*, 102831. [CrossRef]
15. Wang, Z.; Wang, X.; Cao, J.; Yan, X.; Zhang, X.; Wen, H.; Hu, W.; Zhou, Y. Trimeric quaternary ammonium monomer anchored polyamide nanofiltration membrane with high permeate flux and enhanced positive charge density for superior Mg^{2+}/Li^+ separation. *Sep. Purif. Technol.* **2026**, *382*, 135758. [CrossRef]
16. Alshahrani, A.A.; El-Habeeb, A.A.; Alotaibi, N.H.; Shaman, A.A.; Almutairi, W.F.; Alotaibi, S.M.; Hassan, H.M.; Alsohaimi, I.H. Preparation and Characterization of Modified Polysulfone with Crosslinked Chitosan–Glutaraldehyde MWCNT Nanofiltration Membranes, and Evaluation of Their Capability for Salt Rejection. *Polymers* **2022**, *14*, 5463. [CrossRef] [PubMed]
17. Wang, X.; Mao, Y.; Gao, N.; Liao, Y.; Zhang, Y. Ceramic supported polyamide composite nanofiltration membrane with a glutaraldehyde cross-linked chitosan interlayer. *J. Water Process Eng.* **2024**, *68*, 106566. [CrossRef]
18. Borah, H.J.; Gogoi, M.; Das, D.B.; Hazarika, S. Cyclodextrine-glutaraldehyde cross-linked nanofiltration membrane for recovery of resveratrol from plant extract. *J. Environ. Chem. Eng.* **2020**, *8*, 103620. [CrossRef]

19. Wang, W.; Huang, W.-C.; Zheng, J.; Xue, C.; Mao, X. Preparation and comparison of dialdehyde derivatives of polysaccharides as cross-linking agents. *Int. J. Biol. Macromol.* **2023**, *236*, 123913. [CrossRef] [PubMed]
20. Danielli, C.; van Langen, L.; Boes, D.; Asaro, F.; Anselmi, S.; Provenza, F.; Renzi, M.; Gardossi, L. 2,5-Furandicarboxaldehyde as a bio-based crosslinking agent replacing glutaraldehyde for covalent enzyme immobilization. *RSC Adv.* **2022**, *12*, 35676–35684. [CrossRef] [PubMed]
21. Chen, S.; Liu, P.; Li, Z.; Tang, N.; Li, T.; Yu, Y.; Li, F.; Bi, Y. Preparation and Performance of Composite Nanofiltration Membrane Modified by Mussel Coating. *J. Polym. Environ.* **2023**, *31*, 5089–5098. [CrossRef]
22. Lin, W.-T.; Fu, P.; Li, W.-L.; Yu, Y.-H.; Zhang, Z.-L.; Fan, H.-Y.; Huang, X.-J.; Xu, Z.-K.; Wan, L.-S. Cross-linked g-C_3N_4 nanofibers enable thermal stable composite membranes for high-performance loose nanofiltration. *Chem. Eng. J.* **2024**, *494*, 153197. [CrossRef]
23. Xiong, S.; Han, C.; Phommachanh, A.; Li, W.; Xu, S.; Wang, Y. High-performance loose nanofiltration membrane prepared with assembly of covalently cross-linked polyethyleneimine-based polyelectrolytes for textile wastewater treatment. *Sep. Purif. Technol.* **2021**, *274*, 119105. [CrossRef]
24. Sun, T.; Zhu, Z.; Qiu, Z.; Yang, W.; Jiang, Y.; Su, Q.; Zhu, L.; Zhao, Z.; Huang, X.; Xue, Y.; et al. Preparation of hybrid nanofiltration membranes based on Schiff base reaction for hard water softening. *J. Membr. Sci.* **2025**, *717*, 123578. [CrossRef]
25. Sutariya, B.; Karan, S. A realistic approach for determining the pore size distribution of nanofiltration membranes. *Sep. Purif. Technol.* **2022**, *293*, 121096. [CrossRef]
26. Lu, D.; Huang, M.; Zhang, C.; Bu, G.; Li, G.; Geng, Y.; Xu, S.; Xiang, X.; Qian, Y.; Lu, J.; et al. Impact of charge homogeneity on ion selectivity in polyamide membranes. *Nat. Water* **2025**, *3*, 978–991. [CrossRef]
27. Li, M.; Li, J.; Hao, T.; Zhao, D.; Ren, Z.; Li, S.; Wang, M.; Hou, Y. Tailoring the pore size distribution of nanofiltration membranes via surfactants with different alkyl chain lengths: Towards efficient molecular separation. *Sep. Purif. Technol.* **2024**, *339*, 126494. [CrossRef]
28. Cao, X.; Li, Y.; Sun, Y.; Huang, Q.; Chen, K.; Han, X.; Xiao, C.; Song, Y.; Li, X.; Liu, H. Porous graphene/graphene oxide lamellar composite membranes for antibiotic removal. *Sep. Purif. Technol.* **2026**, *404*, 138763. [CrossRef]
29. Li, Y.; Xu, R.; Xu, J.; Ren, Y.; Jiang, Y. High-flux and alkali-resistant nanofiltration membranes via lysine modification for efficient antibiotic desalination. *Sep. Purif. Technol.* **2026**, *395*, 137753. [CrossRef]
30. Zhang, M.; Wang, B.; Xie, M.; Bai, J.; Zhang, R.; Wu, H.; Jiang, Z. In-situ COF-modified nanofibrous substrates for construction of high-flux polyamide nanofiltration membrane. *Chem. Eng. J.* **2025**, *524*, 169263. [CrossRef]
31. Tao, K.; Zhang, Y.; Song, Y.; Chen, Z.; Wang, Y.; Wang, Y.; Tang, J.; Huang, L. PEI-SiO2/GO nanofiltration membrane: Achieved high water permeability and dye rejection rate. *J. Environ. Chem. Eng.* **2025**, *13*, 115011. [CrossRef]
32. Zhao, B.; Chen, G.; Zhao, Z.; Liu, J.; Ren, Q.; Pang, J. Thermally enhanced interfacial interactions for constructing robust PEEK–CMP mixed-matrix nanofiltration membranes for challenging water treatment conditions. *Chem. Eng. J.* **2026**, *546*, 179099. [CrossRef]
33. Liu, Z.; Fang, T.; Jia, S.; Yang, Q.; Wang, C.; Feng, Y. High-selectivity antifouling nanofiltration membranes fabricated via interfacial polymerization using a "fishnet-like" PEG-modified macromolecule. *Sep. Purif. Technol.* **2026**, *409*, 139302. [CrossRef]
34. Liu, G.; Li, C.; Zhang, W.; Luo, W.; Meng, F.; Qi, J.; Zhao, S. Unveiling the role of surface functional groups in organic-inorganic complex fouling of loose nanofiltration membranes for leachate resource recovery. *J. Membr. Sci.* **2026**, *757*, 125962. [CrossRef]
35. Roy, S.; Majumdar, S.; Sahoo, G.C.; Mandal, A.K.; Dey, N.; Mondal, P. Preparation of stable and regenerable ceramic-supported-polymeric composite nanofiltration membrane with high flux and heavy metal removal performance. *J. Water Process Eng.* **2024**, *59*, 104940. [CrossRef]
36. You, M.; Li, W.; Pan, Y.; Fei, P.; Wang, H.; Zhang, W.; Zhi, L.; Meng, J. Preparation and characterization of antibacterial polyamine-based cyclophosphazene nanofiltration membranes. *J. Membr. Sci.* **2019**, *592*, 117371. [CrossRef]
37. Li, Y.-S.; Gao, Y.-W.; Zhu, Y.-K.; Zhang, H.; Zhang, W.-S.; Yin, Y.-H.; Zhang, Y.-X.; Wang, C.-B. Fabrication of self-cleaning nanofiltration membranes through interfacial polymerization using PEI@CoPc monomer for Mg^{2+}/Li^{+} separation. *Chem. Eng. J.* **2024**, *496*, 153807. [CrossRef]
38. Liu, Y.; Dong, X.; Wang, M.; Guo, S.; Zhang, H.; Wang, Z. Modulating interfacial polymerization via 1-methylimidazole as reactive additive for nanofiltration membrane with high-performance. *Desalination* **2023**, *568*, 117021. [CrossRef]
39. Li, J.; Song, Y.; Xu, D.; Zhang, X.; Du, J.; Liu, R.; Zhao, R.; Chen, Q.; Volodine, A.; Dewil, R.; et al. Choline chloride modification of nanofiltration membranes for improving heavy metal ions separation in wastewater. *J. Membr. Sci.* **2024**, *708*, 123079. [CrossRef]
40. Wu, B.; Wang, N.; Lei, J.-H.; Shen, Y.; An, Q.-F. Intensification of mass transfer for zwitterionic amine monomers in interfacial polymerization to fabricate monovalent salt/antibiotics separation membrane. *J. Membr. Sci.* **2022**, *643*, 120050. [CrossRef]
41. Yu, W.-H.; Shen, Y.-J.; Fang, L.-F.; Qiu, Z.-L.; Han, J.; Zhu, B.-K. Tailoring pore size of positively-charged nanofiltration membrane via a facile self-assembly method. *Desalination* **2022**, *542*, 116054. [CrossRef]
42. Wang, Z.; Yan, X.; Qin, R.; Deng, L.; Hu, W.; Wang, Z.; Wang, X. Precision separation of cations in acidic wastewater enabled by an acid-resistant positively charged nanofiltration membrane with high permeability. *J. Water Process Eng.* **2026**, *91*, 110508. [CrossRef]

43. Li, J.; Peng, H.; Liu, K.; Zhao, Q. Polyester Nanofiltration Membranes for Efficient Cations Separation. *Adv. Mater.* **2024**, *36*, 2309406. [CrossRef] [PubMed]
44. Wang, J.; Liang, H.; Liu, T.; Hou, Y.; Chen, Q.; Jia, T.; He, Y. Effects of anions and their coexistence with humic acid on the removal of perfluorobutanoic acid (PFBA) by nanofiltration membrane. *J. Environ. Chem. Eng.* **2026**, *14*, 121937. [CrossRef]
45. Lai, C.; Zhang, W.; Meng, F.; Zhao, S. Sequential monomer immersion guided by density contrast tailors pore structure and surface chemistry in nanofiltration membranes for lithium recovery. *J. Membr. Sci.* **2026**, *758*, 126069. [CrossRef]
46. Shi, D.; Luo, S.; Sun, J.; Xiao, S.; Sun, X.; Qu, Y.; Zeng, R.; Wang, M.; Chen, R.; Tian, Y.; et al. Sandwich-like COF membranes with enhanced chargeability and narrowed nanopores for nanofiltration-based desalination. *J. Membr. Sci.* **2026**, *742*, 125137. [CrossRef]
47. Liu, Y.; Zhang, X.; Chi, M.; Matsuyama, H.; Guo, Y.; Simoens, K.; Volodine, A.; Dewil, R.; Zheng, J.; Dai, Z.; et al. Advancing drinking water safety: Facile fabrication of nanofiltration membrane for enhanced antibiotics removal and efficient water softening. *Desalination* **2024**, *591*, 118024. [CrossRef]
48. Sharma, K.; Akther, N.; Choo, Y.; Zhang, P.; Matsuyama, H.; Shon, H.K.; Naidu, G. Positively charged nanofiltration membranes for enhancing magnesium separation from seawater. *Desalination* **2023**, *568*, 117026. [CrossRef]
49. Liu, Y.; Cen, Q.; Fan, K.; Hu, A.; Yuan, X.; Xia, S. Enhancing nanofiltration membrane selectivity between mineral salts and organic pollutants by sulfonic acid functionalization for drinking water treatment. *J. Membr. Sci.* **2024**, *693*, 122358. [CrossRef]
50. Li, Z.; Wang, X.; Zhang, Q.; Zhai, M.; Yang, S.; Li, X.; Yang, S.; Wu, X.; Song, L. Nitrate rejection of sulfonic acid group incorporated polyethersulfone-type nanofiltration membrane and reutilization of the concentrated solution. *J. Appl. Polym. Sci.* **2023**, *140*, e54616. [CrossRef]
51. Liu, W.; Geng, X.; Li, S.; Zhan, X.; Li, J.; Wang, L.; Lei, J. Preparation of lignosulfonate-based nanofiltration membranes with improved water desalination performance. *Eng. Life Sci.* **2021**, *21*, 417–428. [CrossRef] [PubMed]

Disclaimer/Publisher's Note: The statements, opinions and data contained in all publications are solely those of the individual author(s) and contributor(s) and not of MDPI and/or the editor(s). MDPI and/or the editor(s) disclaim responsibility for any injury to people or property resulting from any ideas, methods, instructions or products referred to in the content.